CHEMISTRY
A EUROPEAN JOURNAL

DOI: 10.1002/chem.200700875

Amphiphilic and Magnetic Properties of a New Class of Cluster-Bearing $[L_2Cu_4(\mu_4\text{-}O)(\mu_2\text{-carboxylato})_4]$ Soft Materials

Rajendra Shakya,[a] Sarmad Sahiel Hindo,[a] Libo Wu,[c] Suolong Ni,[d] Marco Allard,[a] Mary Jane Heeg,[a] Sandro R. P. da Rocha,[c] Gordon T. Yee,[d] Hrant P. Hratchian,*[b] and Cláudio N. Verani*[a]

Dedicated to Professor David Rorabacher on the occasion of his retirement after 50 years of service

Abstract: A general approach toward amphiphilic systems bearing multimetallic clusters and their ability to form Langmuir–Blodgett films is presented. The synthetic strategy to stabilize these clusters involves the use of a ligand (HL) containing an N_2O-donor set and long octadecanoic chains to obtain the carboxylate-supported $[L_2Cu_4(\mu_4\text{-}O)(\mu_2\text{-}OAc)_4]\cdot EtOH$ (**1**) and $[L_2Cu_4(\mu_4\text{-}O)(\mu_2\text{-}OBz)_4]$ (**2**) in which OAc^- and OBz^- represent acetate (**1**) and benzoate (**2**) co-ligands. These species were thoroughly characterized and had their structures solved by X-ray crystallography. We observed that the μ-oxo Cu_4 cluster is antiferromagnetically coupled and used broken-symmetry density functional theory (DFT) calculations to describe the main superexchange pathways of the tetracopper core. We also describe the amphiphilic properties of the ligand and the cluster-containing systems by means of area versus pressure isotherms and show that these cluster-bearing species can be transferred onto solid substrates yielding homogeneous Langmuir–Blodgett films, as characterized by atomic force microscopy and contact angle measurements.

Keywords: amphiphiles · cluster compounds · copper · density functional calculations · Langmuir–Blodgett films · magnetic properties

Introduction

One of the main challenges of modern coordination chemistry is to find ways of translating the considerable amount of information learned from small molecules into useful systems that foster the development of new materials. A main step in this process is the need for small molecules to be organized in highly ordered assemblies and, usually, the need for transfer onto surfaces. The rich chemistry of transition-metal complexes is profuse in systems with well-understood, controllable, and tunable properties, and the incorporation of these motifs into soft materials—thus allowing for interface and surface organization—is highly desirable. Recent advances in the field of metal-containing soft materials point to successful applications toward molecular electronics,[1–4] responsive thin films,[5,6] and hierarchical materials.[7] Other emerging applications focus on metallopolymers[8–10] and dendrimers[11,12] or metallosurfactants[13–15] and mesogens[16–19] taking advantage of the geometric, redox, and magnetic properties of transition-metal centers to build up organized supramolecular architectures based on organic scaffolds. The inclusion of three-dimensional metal clusters

[a] R. Shakya, S. S. Hindo, M. Allard, Dr. M. J. Heeg, Prof. C. N. Verani
Department of Chemistry, Wayne State University
Detroit, MI 48202 (USA)
Fax: (+1) 313-577-2554
E-mail: cnverani@chem.wayne.edu

[b] Dr. H. P. Hratchian
Department of Chemistry
Indiana University
Bloomington, IN 47405 (USA)
Fax: (+1) 812-855-8300
E-mail: hhratchi@indiana.edu

[c] L. Wu, Prof. S. R. P. da Rocha
Department of Chemical Engineering
Wayne State University
Detroit, MI 48202 (USA)

[d] S. Ni, Prof. G. T. Yee
Department of Chemistry
Virginia Polytechnic Institute and State University
Blacksburg, VA 424061 (USA)

Supporting information for this article is available on the WWW under http://www.chemistry.org or from the author.

in soft materials is particularly relevant for molecular electronics for which several oxidation and ground states can become useful for efforts toward information storage. Nonetheless, except for iron–sulfur core dendrimers,[12,20] the approach remains largely unexplored due to intrinsic synthetic challenges. We have shown[16] that this constraint can be overcome by the use of pre-assembled carboxylate-based dimers that interact with properly designed ligands conferring specific properties to the final assembly. Since formation of carboxylate-supported clusters[21,22] has been reported for several first-row metal ions, this methodology constitutes an important starting point. Our interest for transition metals and surface chemistry[23–25] led us to embark on an effort to develop amphiphilic cluster-containing materials capable of film formation. In this article, we present a synthetic strategy for obtaining the Cu_4-cluster-bearing complexes $[L_2Cu_4(\mu_4\text{-}O)(\mu_2\text{-}OAc)_4]\cdot EtOH$ (**1**) and $[L_2Cu_4(\mu_4\text{-}O)(\mu_2\text{-}OBz)_4]$ (**2**) with the new N_2O-terdentate ligand HL (Scheme 1) and μ_2-bridging acetate (μ_2-OAc), benzoate (μ_2-OBz), and μ_4-oxo groups as co-ligands. Both complexes have been exhaustively characterized by spectroscopic and spectrometric techniques and had their structures solved by X-ray crystallography. Since the magnetic properties of multicopper species depends heavily on the cluster geometry,[26] we also investigated the magnetic properties of these complexes both experimentally and by means of molecular calculations. Trying to ascertain the contributions of different magnetic pathways, we present for the first time density functional theory (DFT) calculations on the whole tetracopper core using broken-symmetry approaches. Finally, we describe the amphiphilic properties of the ligand and the cluster-containing systems as pressure versus area isotherms and show that these cluster-bearing species can be transferred onto solid substrates yielding homogeneous Langmuir–Blodgett films characterized by atomic force microscopy and contact angle measurements. The implications of these results toward the design of magnetic and responsive films that incorporate clusters are also offered.

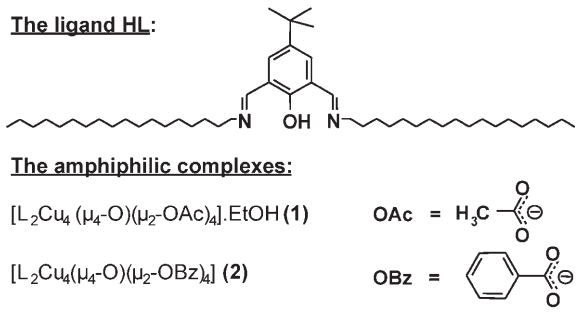

Scheme 1.

Results and Discussion

Synthesis and characterization: The ligand was synthesized by treatment of the precursor 5-*tert*-butyl-2-hydroxyisophtaldehyde and 1-octadecylamine and was analyzed by ^1H NMR and IR spectroscopy as well as ESI mass spectrometry.[16] Complexes **1** and **2** were synthesized by treatment of a solution of the ligand in ethanol with distinct copper salts, and, in both cases, a tetrametallic μ_4-oxo, μ_2-carboxylato bridged core was identified. Copper(II) acetate in a 1:2 ligand-to-metal molar ratio was used to obtain **1**, with the acetate groups acting as μ_2-bridging co-ligands. Few examples of structurally characterized acetato-bridged cores have been reported[27] and the acetate-supported structure is considerably less usual than the equivalent chloro-bridged core.[28–30] When copper perchlorate is added simultaneously with sodium benzoate, complex **2** is obtained with μ_2-bridging benzoate groups replacing the acetate groups observed for **1**. The use of benzoates as co-ligands was intended to validate this synthetic path as a general approach for carboxylate-supported cluster formation. The IR spectra of both **1** and **2** show sharp peaks at about 2920–2850 cm^{-1} corresponding to C–H stretches of the alkyl chains and *tert*-butyl groups. Coordination of the imine nitrogen atoms to the copper is evidenced by a shift of the C=N peak in the ligand to about 1630 cm^{-1} in the complexes. Finally, a sharp peak of medium intensity at 527 cm^{-1} relates to the Cu–O vibration of the μ_4-oxo Cu_4 core.[27,31,32] The microanalyses were in good agreement with the described structures. Further evidence for the stability of the Cu_4 core is given by ESI mass spectrometry (ESI-MS) data taken in methanol, with peaks related to $[M-(OAc)]^+$ for **1** and $[M-(OBz)]^+$ for **2**. These peaks show the expected isotopic distribution associated with copper ions coordinated to N- and O-donors, as shown in Figure 1. The optical behavior of **1** and **2** was studied in dichloromethane. The spectra of both complexes exhibited strong absorption bands at around 380 and 672 nm ($\varepsilon \approx 18000$ and 300 $M^{-1}cm^{-1}$, respectively). The higher energy band is assigned to a $p\pi_{phenolate} \rightarrow d\pi^*_{copper}$ charge-transfer band, whereas the lower energy band is attributed to a d–d transition of the metal,[30,33–35] probably $b_{3g} \rightarrow b_{1g}$ in nature, reflecting an idealized local symmetry C_{4v} expected for each of the square pyramidal copper(II) ions. A weak shoulder at about 800 nm can represent a deviation from this idealized C_{4v} environment either due to the presence of distinct donor sets or due to a square-planar character. The spectrum of **2** in different concentrations is displayed in Figure S1 (Supporting Information) as an illustrative example.

Description of the structures: The crystal structures of both complexes **1** and **2** have been solved and show considerable similarity. The structure of **1** was published elsewhere,[16] and Figure 2 displays the ORTEP diagram for **2** with selected bond lengths and angles. Compound **2** is composed of discrete neutral molecules consisting of two deprotonated ligands (L^-), each delivering a set of three donor atoms N_2O

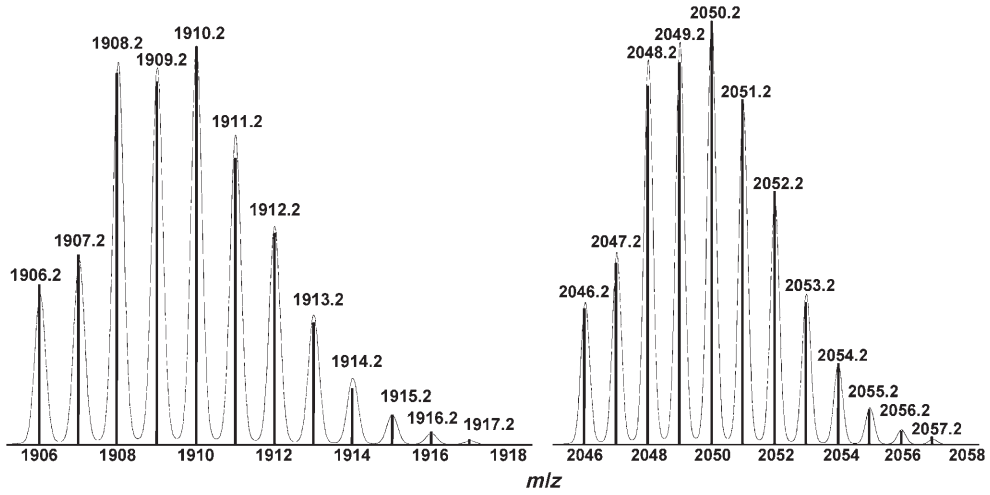

Figure 1. Experimental (bars) and simulated (continuum) ESIMS data for the isotopic cluster referring to $[\mathbf{1}-OAc]^+$ (left) and $[\mathbf{2}-OBz]^+$ (right)

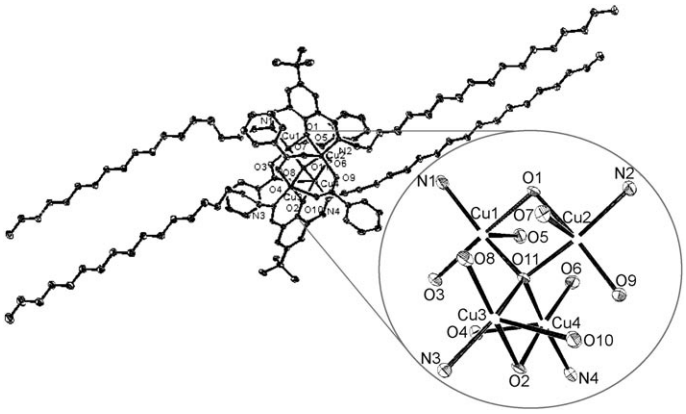

Figure 2. ORTEP at the 50% level representation of the neutral molecule **2**. Copper distances: Cu1–O11: 1.9159, Cu1–O5: 2.3774, N2–Cu2:1.9784, Cu2–O9: 1.9373, Cu1–O3: 1.9498, Cu1–N1: 1.983, Cu1–O1: 2.0004, Cu1–Cu2: 3.0064, Cu1–Cu3: 3.2525, Cu1–Cu4: 3.1935, Cu2–Cu3: 3.1723, Cu2–Cu4: 3.1908, Cu3–Cu4: 2.9975, Cu2–O(11): 1.9134, Cu2–O1: 1.9864, Cu2–O7: 2.2574, Cu3–O11: 1.9379, Cu3–O8: 1.9452, Cu3–N3: 1.9829, Cu3–O2: 1.9859, Cu3–O10: 2.3507, Cu4–O11: 1.9173, Cu4–O6: 1.9383, Cu4–N4: 1.989, Cu4–O2: 1.9922, Cu4–O4: 2.2678 Å; average distances: C–C in Ph:1.411, C–C in Ph:1.403, C–C in C18H37 chains: 1.527, C–C in OBz: 1.387 Å; selected angles: N2–Cu2–O7 :89.63, N4–Cu4–O11 :164.46, Cu1–O1–Cu2:97.89, Cu3–O2–Cu4:97.79, Cu3–O11–Cu1:115.12, Cu3–O11–Cu4:102.06, Cu1–O11–Cu4:112.84, Cu3–O11–Cu2:110.91, Cu1–O11–Cu2:103.46, Cu4–O1–Cu2: 112.81°.

to a cluster of four copper(II) centers μ_4-bridged by a distorted tetrahedral oxygen atom (O11).[27,29,36] Two benzoate groups link Cu1 and Cu4 and another two link Cu2 and Cu3, with each benzoate showing alternating short (1.94 Å) and long (2.35 Å) Cu–O bonds. The four $Cu-N_{imine}$ bonds are consistently found at 1.98 Å, fostering a five-coordinate geometry. A square-pyramidal geometry can be inferred from τ values[37] ranging from 0.011 to 0.103. Interestingly, the halogeno-bridged counterparts tend to have a more pronounced trigonal-bipyramidal character.[30]

The main differences between **1** and **2** relate to the substitution of the μ_2-bridging acetato by benzoato ligands, with an apparent distortion of the organic scaffold of the latter resulting from the presence of the bulky benzoate rings. However, keeping in mind that both structures are comparable in quality ($R_1 = 0.0531$ and 0.0497 for **1** and **2**, respectively), we observe similarities between both cores: All $Cu-O_{phen}$ bonds are found between 1.98 and 1.99 Å, the $Cu-O_{oxo}$ bonds range only from 1.98 to 2.00 Å, and changes in angles are also minimal (Figures S2 and S3 in the Supporting Information), with the most pronounced difference being a mere 2° in the intradimer Cu-O-Cu values.

Magnetic susceptibility: Temperature-dependent magnetization data was collected from 300 to 1.8 K in order to evaluate the nature and magnitude of the magnetic coupling superexchange pathways in **1** and **2**, as well as the potential influence of the long octadecyl chains. Figure 3 shows the χ versus T magnetization plot for **2**, while data for **1** is shown in Figure S4 (in the Supporting Information). Both compounds exhibit a dominant antiferromagnetic behavior, and we have fit the data to the simplified model suggested by Haase, Krebs, et al.,[29] under which the tetranuclear copper

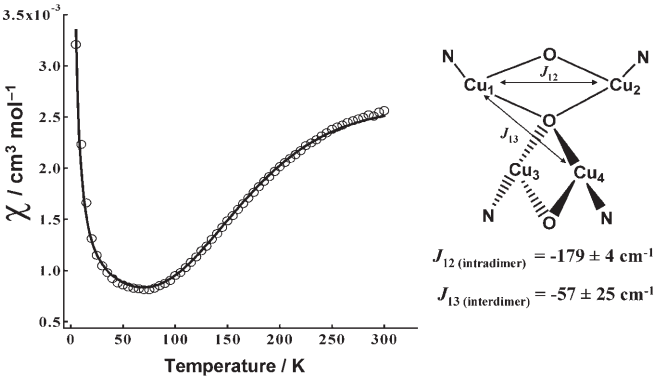

Figure 3. Magnetic susceptibility for **2**: Inset: Coupling scheme.

core is treated as a dimer of Cu_2O_2 dimers. The approach is depicted on the right hand side of Figure 3 along with the magnetic data with the dimer indicated in blue. Four possible superexchange pathways must be considered: The Cu-O_{phen}-Cu and Cu-O_{oxo}-Cu intradimer interactions and the interdimer Cu-O_{oxo}-Cu and Cu-OAc-Cu interactions. Since each μ_2-bridging benzoate ligand shows a short and a long Cu–O bond, the potential coupling through these groups is considered to be irrelevant. The spin Hamiltonian for **1** and **2** is described by Equation (1), and the magnetic susceptibility data [Eq. (2)] were fit by non-linear least-squares methods, corrected for a typographical error previously published.[29] The inclusion of the second term accounts for the magnetic susceptibility from monomeric Cu^{II} impurities at a mole fraction given by x_p. The third term is the temperature-independent paramagnetism (TIP). All other constants in Equation (2) have their usual meanings and values.

$$H = -2[J_{12}(S_1 \cdot S_2 + S_3 \cdot S_4) + J_{13}(S_1 \cdot S_3 + S_1 \cdot S_4 + S_2 \cdot S_3 + S_2 \cdot S_4)] \quad (1)$$

This expression considers two main magnetic interactions given by J_{12} and J_{13}. The former describes the intradimer coupling constant, whereas the latter takes into account the interdimer coupling through the μ_4-oxo bridge, as indicated above. In using Equation (2), we have chosen to fix the g value at 2.19, a reasonable value for the Cu^{II} ion. It leaves four adjustable parameters, and, for **1**, the best fit of the data yields $J_{12} = -212 \pm 5\ cm^{-1}$, $J_{13} = -98 \pm 28\ cm^{-1}$, $x_p = (2.34 \pm 0.05)\%$, $TIP = 0.00098 \pm 0.00001\ cm^3 mol^{-1}$, and $R = 0.0795$, in which $R = \Sigma[(\chi_{calcd} - \chi_{exptl})/\chi_{exptl}]^2$.

The fit to the data is well within acceptable limits. As reported previously,[29] the uncertainty in the value for J_{13} is substantial, because of the lack of data at temperatures above 300 K. At this point, we are not able to collect data at high temperatures. Similarly, for **2**, the fit yields $J_{12} = -179 \pm 4\ cm^{-1}$, $J_{13} = -57 \pm 25\ cm^{-1}$, $x_p = (3.05 \pm 0.06)\%$ and $TIP = 0.00061 \pm 0.00002\ cm^3 mol^{-1}$, which are consistent with the values found for the acetate analogue **1**. The fit is slightly better with $R = 0.0362$. Comparison of the data for **1** and **2** shows that the relatively greater magnitude of J_{12} compared to J_{13} is in agreement with previously published data, as shown by selected examples[27,29,30,32] in Table T1 (in the Supporting Information). A difference of about $30\ cm^{-1}$ in the coupling constants points to stronger coupling in **1** than in **2**. As mentioned in the previous section, close examination of the two molecular structures reveals minimal differences that should lead to similar superexchange pathways and do not justify the observed coupling values. These differences in J_{12} and J_{13} between the two compounds might be an artifact resulting from the lack of data at high temperatures. On the other hand, a previous article[16] on the mesomorphic properties of **1** showed that vicinal imine bonds, about 3.40 Å apart, appear to contribute to columnar formation. These interactions are suggestive of some degree of π-stacking and are absent in **2**. One can suggest that this imine overlap can reinforce some long-order coupling phenomenon. Having collected the experimental data concerning the magnetic susceptibility of the complexes, we turned to density functional theory calculations to provide an accurate molecular orbital description of the superexchange pathways that facilitate the observed spin–spin couplings.

Electronic structure calculations and analysis: Calculations on Cu_4 clusters are limited to a few examples of cubane-like structures[38] and—to the best of our knowledge—are nonexistent for μ_4-oxo-bridged scaffolds. To make our DFT calculations more tractable, we employed a structural model for **1** and **2**, shown in Figure 4. This model preserves the central Cu_4O core, the N_2O_{phen} ligand framework connecting the metal centers by two Cu_2 units; the bridging formate groups (COO^-) replace the original acetate and benzoate groups. The optimized structure belongs to the D_2 point

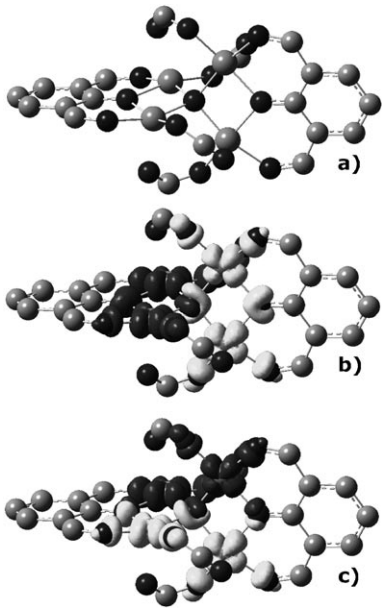

Figure 4. a) 3D rendering of the computational model, b) spin density plot for the broken-symmetry interdimer coupled state, and c) equivalent spin density plot for the intradimer state. Mulliken spin densities (electrons) for the interdimer coupled state: Cu1 = 0.74, Cu2 = 0.74, Cu3 = −0.74, Cu4 = −0.74, O = 0.00, O_{phen12} = 0.09, O_{phen34} = −0.09. Mulliken spin densities (electrons) for the intradimer coupled state: Cu_1 = −0.72, Cu_2 = 0.72, Cu_3 = −0.72, Cu_4 = 0.72, O = 0.00, O_{phen12} = 0.00, O_{phen34} = 0.00.

$$\chi_m = (1 - x_p)\frac{Ng^2\beta^2}{kT}\frac{10\exp(2J_{12}/kT) + 2\exp(-2J_{12}/kT) + 4\exp(-2J_{13}/kT)}{5\exp(2J_{12}/kT) + 3\exp(-2J_{12}/kT) + \exp(-4J_{12}/kT) + 6\exp(-2J_{13}/kT) + \exp(-4J_{13}/kT)} + x_p\frac{Ng^2\beta^2}{3kT}S(S+1) + TIP \quad (2)$$

group and the bond lengths and angles are in good agreement with the crystallographic data for **2**. Exceptions are the Cu–$O_{formate}$ bonds and intradimer Cu-(μ_4-O)-Cu angles, which, in the DFT optimized structure, are 0.06–0.18 Å and ~10° smaller than the corresponding parameters in the crystal structure of **2**. The shorter distances are attributed to the weak nature of the bonding interaction that may be overestimated with the level of theory employed here (see the Experimental Section below for details), whereas the smaller angles are attributed to the absence of the long alkyl chains that may distort the angles between the two Cu_2 dimers in **2**. Superexchange pathways were studied by converging broken-symmetry open-shell singlet states corresponding to the expected spin configurations. Two states corresponding to the inter- and intradimer coupled configurations have been considered. It is worth noting that the benzoate groups do not engage in the spin couplings and that two possible and equivalent intradimer states are present. We arbitrarily chose the intradimer state in which copper centers bridged by the same two formate groups have parallel spins. Before evaluating the results relevant for superexchange pathways, the electronic structure that is predicted from qualitative molecular orbital theory must be considered given that two Cu centers have one unpaired α electron each, while the other two Cu centers have one unpaired β electron each, the symmetry of the open-shell singlet wavefunctions of the D_2 model structure is C_2 for both the inter- and intradimer coupling cases. Since the local coordination sphere at each metal atom is square pyramidal, the unpaired electron at each site occupies the $d_{x^2-y^2}$ orbital. Figures 4b and c include the spin density difference plots for the calculated broken-symmetry states; the Mulliken spin densities support the characterization of these as correct broken-symmetry open-shell singlet states. Furthermore, calculation of the spatial overlap of α and β densities shows that 2.0 α and 2.0 β electrons are unpaired.

From the spin densities, we noticed that the μ_4-O bridge is involved with both spin-coupling pathways. Indeed, the central oxygen atom is the communication source for opposing copper spin centers in the interdimer state, and it plays a key role in the superexchange pathway in the intradimer state. Because the spin densities have C_2 symmetry, the magnetic molecular orbitals are delocalized across all four metal atoms. From a practical point of view, the symmetry of our broken-symmetry states makes it difficult to identify, simply from inspection, the magnetic molecular orbitals that are responsible for the computed spin density differences as well as the experimentally observed magnetism. Instead, we have evaluated the spatial overlap of all α molecular orbitals with the β density and vice versa. Figures 5a and b show molecular orbitals with less than 0.90 e^- overlap with the opposite spin density. In the interdimer case (Figure 5a), the HOMO and HOMO−5 are the important contributors to the spin coupling with 0.36 and 0.51 e^- opposite spin overlaps, respectively. For the intradimer case (Figure 5b), the HOMO, HOMO−1, HOMO−2, and HOMO−4 are important contributors to the spin coupling with 0.56, 0.76, 0.80, and 0.63 e^- opposite spin overlaps, respectively. Mulliken percent character values (over selected atomic centers) for these orbitals are given in Table 1. As might be expected, the α/β molecular orbital pairs are symmetric in their relative compositions. For example, the interdimer coupled state α-HOMO is comprised of $d_{x^2-y^2}$ on two Cu centers, d_{z^2} on the two other Cu centers, and a p orbital on the central μ_4-O. The β-HOMO is comprised of the same p orbital on the central μ_4-O and Cu $d_{x^2-y^2}$ and d_{z^2} orbitals on the metal

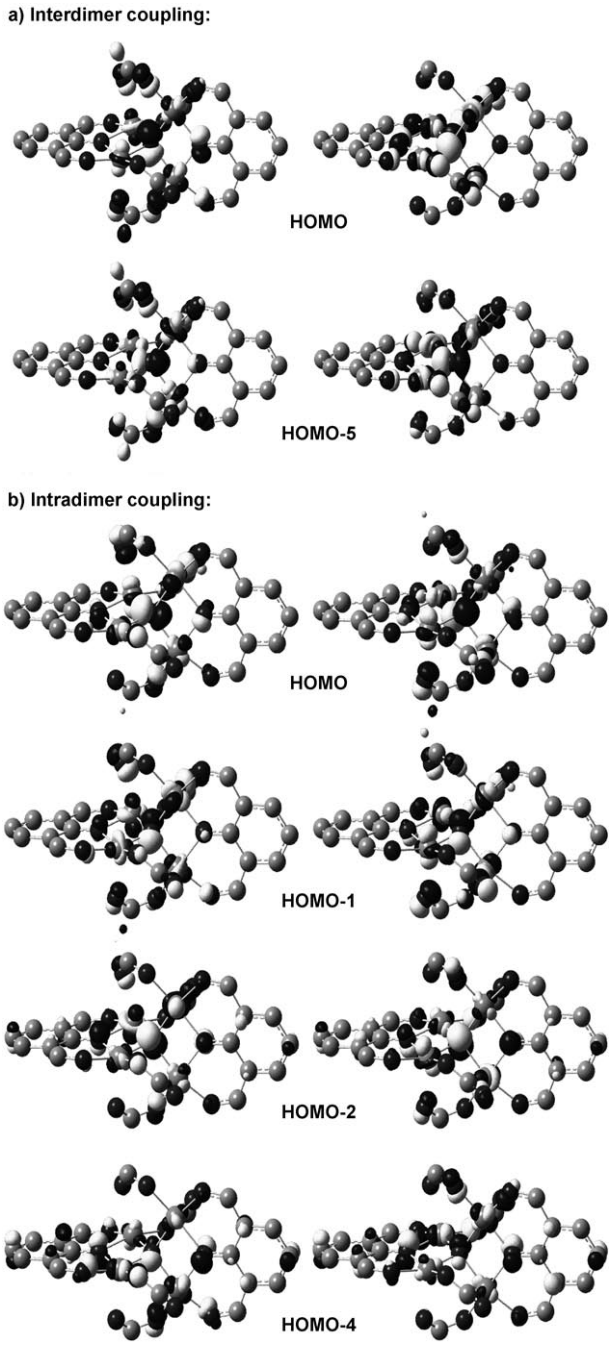

Figure 5. Selected molecular orbital renderings from the broken-symmetry coupled states: a) inter- and b) intradimer. α orbitals are shown on the left; β orbitals are shown on the right.

Table 1. Mulliken percent character values for selected HOMO frontier orbitals for the inter- and intradimer-coupled broken-symmetry states.

MO		% Population						
		Cu1	Cu2	Cu3	Cu4	O	$O_{phen\text{-}1,2}$	$O_{phen\text{-}3,4}$
interdimer								
HOMO	α	10.4	10.4	6.9	6.9	19.7	6.8	0.6
	β	6.9	6.9	10.4	10.4	19.7	0.6	6.8
HOMO−5	α	13.8	13.8	7.6	7.6	14.2	1.5	0.1
	β	7.6	7.6	13.8	13.8	14.2	0.1	1.5
intradimer								
HOMO	α	10.5	8.8	10.5	8.8	14.9	3.2	3.2
	β	8.8	10.5	8.8	10.5	14.9	3.2	3.2
HOMO−1	α	12.4	7.8	12.4	7.8	10.4	1.9	1.9
	β	7.8	12.4	7.8	12.4	10.4	1.9	1.9
HOMO−2	α	10.5	5.9	10.5	5.9	12.3	4.7	4.7
	β	5.9	10.5	5.9	10.5	12.3	4.7	4.7
HOMO−4	α	9.3	4.1	9.3	4.1	4.8	6.5	6.5
	β	4.1	9.3	4.1	9.3	4.8	6.5	6.5

pairs opposite the α-HOMO. The relative compositions quantify this symmetry. In the interdimer coupled state, the Cu1 and Cu2 orbitals make up 10.4% of the α-HOMO, and the Cu3 and Cu4 orbitals make up 6.9% of α-HOMO. For the β-HOMO, 6.9% of the orbital character comes from the Cu1 and Cu2 orbitals, and 10.4% comes from the Cu3 and Cu4 orbitals. Again, this symmetry results from a description of the total complex as a dimer of dimers. All of the magnetic molecular orbitals can be described as symmetric or antisymmetric combinations of Cu_2 dimer fragment orbitals interacting through the central μ_4-O bridge. The μ_4-O orbitals hybridize to σ-bonds with the dominant Cu_2 dimer orbitals. In most cases, the μ_4-O bridge also forms a σ-bond with the other Cu_2 dimer. However, the character of the interactions between the μ_4-O and this Cu_2 dimer in the interdimer HOMO and the intradimer HOMO−1 and HOMO−2 are best described as nonbonding. Interestingly, d_{z^2} orbitals on the minor Cu_2 dimer in the interdimer HOMO and intradimer HOMO−2 have hybridized with other d orbitals to tip slightly off their local z axes. As a result, the interactions with the μ_4-O in these two molecular orbitals do have some π-bonding character, albeit quite small.

In the interdimer coupled state, the calculations show that the μ_4-O is the sole center facilitating spin coupling, while in the intradimer coupled state the phenolate-O atoms act together with the μ_4-O to couple Cu spins. Although phenolate-O atoms engage in the intradimer superexchange pathway, the μ_4-O atom is the largest individual contributor to three of the magnetic molecular orbitals. The exception is the intradimer HOMO−4, in which all three O atoms are nearly equal participants. The spatial overlap between α and β spin orbitals is greatest for the intradimer coupled state. Because the α/β spatial overlap is related to the coupling strength, this indicates that the intradimer coupling should be stronger than for the interdimer case. This is further supported by the DFT energy difference between these states, which favors the intradimer state by more than 100 cm^{-1}. These results qualitatively agree with our magnetization data discussed above. Further DFT studies of specific structure–superexchange correlations are ongoing and will be reported in future work.

Amphiphilic properties and Langmuir–Blodgett film formation: The amphiphilic properties of the ligand HL and the complexes **1** and **2** are displayed as surface pressure (Π in $mN\,m^{-1}$) versus area per molecule (A in $Å^2$) in Figure 6.

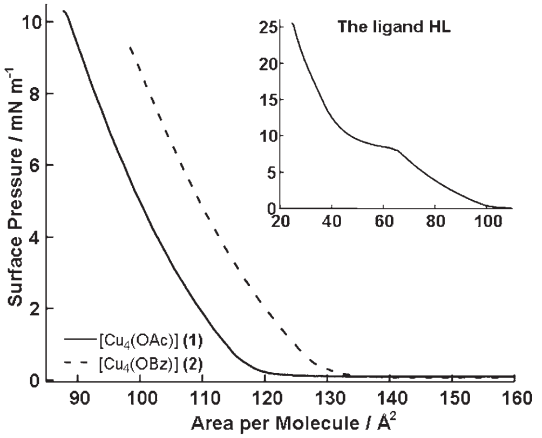

Figure 6. Surface pressure versus area per molecule isotherms at the air–water interface for the ligand HL, **1**, and **2**.

These isotherms give information about the two-dimensional behavior of the resulting amphiphilic film, the limiting area per molecule (A_{lim}), the collapse pressure (Π_c), and the area at the collapse of the monolayer (A_c). The film remaining after solvent evaporation has the thickness of a single molecule and is referred to as a monolayer. As the barriers of the trough are compressed, the tension (γ) of the air–water interface in the presence of the ligand or complexes decreases relative to that of the bare air–water interface (γ_0), resulting in an increase in Π ($=\gamma_0-\gamma$). The isotherms for the ligand, and complexes **1** and **2** were obtained and revealed amphiphilic behavior for all species. One of the main concerns for cluster-containing amphiphilic molecules is that they should keep their composition at the air–water interface without disassembling into smaller species. In order to ensure consistency, each isotherm was repeated at least three times; excellent reproducibility was attained for both HL and the complexes **1** and **2**. Overnight experiments in which the monolayers were left resting at the interface for extended periods of time gave consistent areas per molecule. Similarly, ESI-MS data of aged solutions of **1** and **2** in dichloromethane reproduced the behavior observed for fresh samples reinforcing the notion that the tetracopper clusters are stable. The molecules of the protonated ligand start interacting with each other at the air–water interface at about 100 $Å^2 molecule^{-1}$ forming an expanded phase that is followed by a phase transition at about 65 $Å^2 molecule^{-1}$. This transition may be due to rearrangement of the alkyl chains that favor an alignment needed for a condensed phase. The

monolayer of the ligand exhibits a moderate collapse pressure at 25 mN m^{-1}. The critical area $A_c = 47$ Å^2 molecule^{-1} can be determined by extrapolating the Π versus A curve at its steepest slop before the collapse to zero pressure at which it intercepts the x axis.[5] The A_c value determined for the ligand is much larger than the 20 Å^2 molecule^{-1} observed for heptadecanoic acid,[39] but closer to the area occupied by more voluminous species like *cis*-13-docosenoic acid (eruric acid, $C_8H_{17}CH{=}CHC_{11}H_{22}COOH$, 38 Å^2 molecule^{-1}) and dimyristolphosphatidic acid (51 Å^2 molecule^{-1}).[40] The presence of bulky tertiary butyl groups is likely to play a role in the packing of the ligand. Ongoing research in our labs focuses on methyl- and halogeno-substituted ligands.

The individual molecules for both **1** and **2** start interacting at the air–water interface at about 127 and 137 Å^2 molecule^{-1}, respectively, but **1** shows a more condensed monolayer than **2** throughout. The molecules of **1** in the monolayer can be compressed to an average area of about 110 Å^2 collapsing at a pressure of 10.25 mN m^{-1}. Molecules of **2** in the monolayer can be compressed to 121 Å^2 molecule^{-1} collapsing at 9.4 mN m^{-1}. When **1** is compared to the ligand, an increase of about 63 Å^2 molecule^{-1} in the A_c value is observed. It is known that a maximum increase of about 10 Å^2 molecule^{-1} is observed upon complexation of the Cu^{II} ion.[41] Thus, the magnitude of the increase observed from HL to **1** reinforces the presence of a cluster. Similarly, the behavior observed for **2** reflects the presence of a bulkier core associated with the four benzoate groups, which prevents the molecules from coming in closer proximity. It is useful to compare these areas with other bulky species, such as substituted fullerenes.[42] In the case of 1-*tert*-butyl-9-hydrofullerene-60, the observed limiting areas of about 20 Å^2 molecule^{-1} clearly indicate the presence of multilayers and the fact that up to six molecules can tumble over each other. In this regard, the large areas observed for **1** and **2** reinforce the notion of monolayer formation. The relatively low collapse pressures can be tentatively attributed to the presence of four hydrophobic alkyl chains, each with its origin about 90° from one another, that envelope the Cu_4-cluster decreasing the hydrophilic character of the core (Scheme 2).

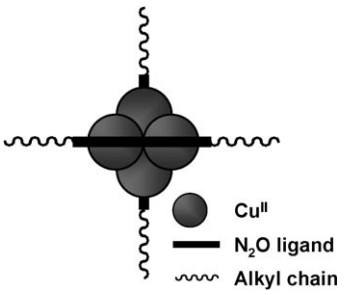

Scheme 2.

It is established that incorporation of salts increases the ionic strength of the subphase, influencing the properties of the monolayers and, in general, improving the order of charged fatty acid surfactants and metallosurfactants.[43] In the particular case of fatty acids, the order enhancement comes through coordination of the acetate head groups with the metal cations; however, more recently, it has been observed that changes in the A_c value may be related to charge.[44] This dependence seems related to the design of the metallosurfactant. To assess the effect of metal salts on the amphiphilic behavior of **1** and **2**, sodium chloride was added to the water subphase. A minor increase in collapse pressures to about 11 mN m^{-1} was observed and associated with a considerable increase in area per molecule. In the presence of the electrolyte, compound **1** expands its structure considerably, occupying an area of 175 Å^2 molecule^{-1}, whereas **2** shows a rather moderate expansion to 150 Å^2 molecule^{-1}. Since the complexes are neutral, the expansions observed are attributed to strong ion–dipole interactions and by ion-induced dipole interactions associated with minor structural rearrangements. The less shielded neutral core of acetate-containing **1** is more susceptible to such repulsions, while the benzoate groups around **2** may insulate the Cu_4 core more effectively.

The monolayers of **1** and **2** in pure water are readily transferred onto mica substrates with deposition ratios close to unity and forming homogeneous Langmuir–Blodgett films. Monolayers of **1** and **2** were deposited at 8 mN m^{-1} and are shown in Figure S5 (see the Supporting Information). Equilibrium contact angle (θ) measurements of 84 and 85° were observed for the monolayers of **1** and **2**, respectively, in clear contrast with the $\theta = 0°$ for the hydrophilic mica substrate. Several attempts to scratch the surface of the transferred film were unsuccessful, suggesting that the monolayers are strongly attached to the mica substrate.

Conclusions

In this paper we presented data regarding μ_4-oxo tetracupric cores supported by four μ_2-carboxylate groups and two amphiphilic and deprotonated L^- ligands that contain an N_2O-donor set and long C_{18}-alkyl chains. Carboxylate sources are acetates for **1** and benzoates for **2**, and together these species validate a new general approach to synthesize μ_4-oxo-bridged metal clusters. These cluster-bearing species act as metallosurfactants showing moderate collapse pressures and allowing for Langmuir film formation at the air–water interface with subsequent transfer onto a solid substrate. The resulting Langmuir–Blodgett films showed remarkable homogeneity and were characterized by atomic force microscopy and contact angle measurements. The magnetic properties of these complexes were studied both experimentally and theoretically and show that antiferromagnetic interactions dominate the coupling scheme and that the superexchange mechanisms rely heavily on the Cu-oxo-Cu pathway. Ongoing research in our labs involves the full characterization of these films, as well as the systematic use of alternative side chains varying in length and nature, and the formation

of [Cu_4-bridge-Cu_4-bridge] extended systems by the replacement of one or more acetate co-ligands by terephtalic acid, aiming at extended magnetic materials with amphiphilic properties.

Experimental Section

Materials and methods: Reagents and solvents were used as received from commercial sources and ethanol was distilled over CaH_2. IR spectra were measured as KBr pellets on a Tensor 27 FTIR-Spectrophotometer. ^1H NMR spectra were measured using a Varian 400 MHz instrument. Mass spectrometry in ESI(positive) mode was measured in a Micromass QuattroLC triple quadrupole mass spectrometer. Experimental assignments were simulated based on peak position and isotopic distributions. Elemental analyses were performed by Midwest Microlab, Indianapolis, IN. UV/Vis spectra of 1.0×10^{-4} M solutions of the samples in dichloromethane were performed in a Cary 50 spectrometer. Magnetic measurements as a function of temperature were performed from 1.8 to 300 K for **1** and **2** on a 5 or 7 T Quantum Design MPMS SQUID magnetometer. Diamagnetic corrections were attained with Pascal's constants, and the diamagnetic susceptibility of the sample holder was also taken into account.

X-ray structural determination for 2: Diffraction data were measured on a Bruker X8 APEX-II kappa geometry diffractometer with Mo radiation and a graphite monochromator at 100 K. Frames were collected as a series of sweeps with the detector at 40 mm and 0.3° between each frame. Frames were recorded for 5 s. Crystals of **2** [$C_{124}H_{194}N_4O_{11}Cu$] grew as green plates, and the sample used for data collection was approximately $0.32\times0.23\times0.14$ mm^3. A total of 3190 frames were collected yielding 107490 reflections, with 29020 of which being independent. Hydrogen positions were placed in calculated positions. No solvent or ions were present in the crystal. Thermal parameters increase along the length of the pendant chains. The asymmetric unit contains one neutral molecule. Complex **2**: Formula, $C_{126}H_{194}N_4O_{11}Cu_4$; M_r, 2170.99 amu; space group $P\bar{1}$; cell constants $a=13.0185(5)$, $b=19.9429(8)$, $c=24.3042(9)$ Å, $\alpha=98.926(2)$, $\beta=101.618(2)$, $\gamma=100.642(2)°$; $V=5951.9(4)$ Å^3; $Z=2$; $T=100(2)$ K; $\lambda=0.71073$ Å; $\rho_{calcd}=1.211$ g cm^{-3}; $\mu=0.763$ mm^{-1}; $R(F)=4.97\%$; $Rw(F)=13.16\%$.

Electronic structure calculations: Becke's three-parameter hybrid exchange functional was used with the nonlocal correlation functional of Perdew and Wang for all DFT calculations.[45] The Pople style 3-21G basis set was used on C and H atoms, while the 6-31G(d) basis set was used on N, O, and Cu centers. The model system geometry was optimized by standard methods.[46] The geometry was found on the high-spin, $M_s=5$, potential-energy surface. Calculations were carried out with the GAUSSIAN suite of electronic structure programs.[47] For all broken-symmetry calculations, the UB3PW91/6-31G(d) model chemistry was used, and stabilities[48] of all wave functions were verified.

Surface pressure versus area isotherms and Langmuir–Blodgett films: Monolayer experiments were carried out by using an automated KSV minitrough at 23.0 ± 0.5 °C. Ultrapure water (Barnstead NANOpure) with a resistivity of 17.5–18 MΩ cm^{-1} was used in all experiments. Impurities present at the surface of the freshly poured aqueous subphase were removed by vacuum after the compression of the barriers without surfactant. Spreading solutions were prepared in spectra grade chloroform. A freshly prepared surfactant solution (30 μL) with a known concentration (1.0 mg mL^{-1}) was then spread on the clean aqueous subphase. The system was allowed to equilibrate for about 15 min before monolayer compression. The Π versus A isotherms were obtained at a compression rate of 5 mm min^{-1}. The Wilhelmy plate method (paper plates 20 mm × 10 mm) was used to measure the surface pressure. The selected graph represents the results of at least three independent measurements with excellent reproducibility. Monolayers (single layer per substrate) were transferred onto $40\times20\times0.08$ mm^3 mica substrates (Ted Pella, Inc) at different target pressures.

Atomic force microscopy and contact angle measurements: The surface topography of freshly prepared Langmuir–Blodgett (LB) films on mica substrates was examined by using a PicoSPM LE (Molecular Image Corp) AFM under tapping mode operation with a BS-Multi 75 (Budgetsensors, Inc) silicon cantilever. The static contact angle of the modified substrates was determined in order to follow the quality of the film. Contact angles were determined on a goniometer (KSV CAM 200) equipped with a CCD camera. All data were collected at room temperature.

Syntheses: The syntheses of the ligand and **1** were reported previously.[16]

$[L_2Cu_4(\mu_4\text{-}O)(\mu_2\text{-}OBz)_4]$ (2): A solution of HL (0.35 g, 0.5 mmol) in ethanol (40 mL) was treated with a solid sample of $Cu(ClO_4)_2\cdot6H_2O$ (0.37 g, 1.0 mmol) followed by addition of sodium benzoate (0.29 g, 2.0 mmol). The resulting green solution was gently heated for 1 h, cooled to room temperature, and filtered. Crystals suitable for X-ray analysis were obtained after slow evaporation of the solvent. Yield = 78%; m.p. = 78–81 °C; IR (KBr): $\tilde{\nu}=1629$ ($\nu_{C=N}$), 2852–2922 cm^{-1} (ν_{C-H} from alkyl chain and *tert*-butyl); ESI$^+$ in MeOH: m/z: 2550.5 $[M-OBz]^+$; elemental analysis calcd (%) for $C_{124}H_{194}Cu_4N_4O_{11}$: C 68.60, H 9.01, N 2.58; found: C 68.31, H 9.09, N 2.52.

Acknowledgements

C.N.V. thanks the Wayne State University, the Donors of the ACS-Petroleum Research Fund (Grant No. 42575-G3), the Nano@Wayne initiative (Fund-11E420), and the National Science Foundation (Grant CHE-0718470), G.T.Y. acknowledges the National Science Foundation (Grant CHE-023488), S.R.P.R. thanks the National Science Foundation (Grant CTS-0553537), H.P.H. acknowledges the Indiana University (Department of Chemistry) Ernest R. Davidson Fellowship for financial support, and R.S. thanks the WSU-Institute for Manufacturing Research for support. Prof. K. Raghavachari (IU) is thanked for insightful discussions and Dr. L. Hryhorczuk (WSU) is kindly acknowledged for the measurement of the mass analyses.

[1] a) R. A. Wassel, C. B. Gorman, *Angew. Chem.* **2004**, *116*,5230; *Angew. Chem. Int. Ed.* **2004**, *43*, 5120; b) C. Joachim, J. K. Gimzewski, A. Aviram, *Nature* **2000**, *408*, 541.
[2] P. J. Low, *Dalton Trans.* **2005**, 2821.
[3] J. Park, A. N. Pasupathy, J. I. Goldsmith, C. Chang, Y. Yaish, J. R. Petta, M. Rinkoski, J. P. Sethna, H. D. Abruña, P. L. McEuen, D. C. Ralph, *Nature* **2002**, *417*, 722.
[4] S. Flores-Torres, G. R. Hutchison, L. J. Soltzberg, H. D. Abruña, *J. Am. Chem. Soc.* **2006**, *128*, 1513.
[5] D. R. Talham, *Chem. Rev.* **2004**, *104*, 5479.
[6] a) A. Pasc-Banu, C. Sugisaki, T. Gharsa, J.-D. Marty, I. Gascon, M. Krämer, G. Pozzi, B. Desbat, S. Quici, I. Rico-Lattes, C. Mingotaud, *Chem. Eur. J.* **2005**, *11*, 6032; b) M. Clemente-León, E. Coronado, C. J. Gómez-García, C. Mingotaud, S. Ravaine, G. Romualdo-Torres, P. Delhaès, *Chem. Eur. J.* **2005**, *11*, 3979; c) D. Y. Takamoto, E. Aydil, J. A. Zasadzinski, A. T. Ivanova, D. K. Schwartz, T. Yang, P. S. Cremer, *Science* **2001**, *293*, 1292.
[7] Y. Bodenthin, U. Pietsch, H. Mohwald, D. G. Kurth, *J. Am. Chem. Soc.* **2005**, *127*, 3110.
[8] S. J. Rowan, J. B. Beck, *J. Am. Chem. Soc.* **2003**, *125*, 13922.
[9] J. L. Bender, P. S. Corbin, C. L. Fraser, D. H. Metcalf, F. S. Richardson, E. L. Thomas, A. M. Urbas, *J. Am. Chem. Soc.* **2002**, *124*, 8526.
[10] I. Manners, *Science* **2001**, *294*, 1664.
[11] D. R. Blasini, S. Flores-Torres, D.-M. Smilgies, H. D. Abruña, *Langmuir* **2006**, *22*, 2082.
[12] T. L. Chasse, R. Sachdeva, Q. Li, Z. Li, R. J. Petrie, C. B. Gorman, *J. Am. Chem. Soc.* **2003**, *125*, 8250.
[13] S. Kraus, D. Mandler, *Langmuir* **2006**, *22*, 7462.
[14] P. C. Griffiths, I. A. Fallis, D. J. Willock, A. Paul, C. L. Barrie, P. M. Griffiths, G. M. Williams, S. M. King, R. K. Heenan, R. Görgl, *Chem. Eur. J.* **2004**, *10*, 2022; King, R. K. Heenan, R. Görgl, *Chem. Eur. J.* **2004**, *10*, 2022.

[15] J. Bowers, K. E. Amos, D. W. Bruce, R. K. Heenan, *Langmuir* **2005**, *21*, 5696.
[16] R. Shakya, P. H. Keyes, M. J. Heeg, A. Moussawel, P. A. Heiney, C. N. Verani, *Inorg. Chem.* **2006**, *45*, 7587.
[17] E. Terazzi, S. Suarez, S. Torelli, H. Nozary, D. Imbert, O. Mamula, J.-P. Rivera, E. Guillet, J.-M. Bénech, G. Bernardinelli, R. Scopelliti, B. Donnio, D. Guillon, J.-C. Bünzli, C. Piguet, *Adv. Funct. Mater.* **2006**, *16*, 157.
[18] a) K. Binnemans, *Chem. Rev.* **2005**, *105*, 4148; b) K. Binnemans, K. Lodewyckx, B. Donnio, D. Guillon, *Chem. Eur. J.* **2002**, *08*, 1101.
[19] a) J. L. Serrano, T. Sierra, *Coord. Chem. Rev.* **2003**, *242*, 73; b) J. L. Serrano, T. Sierra, *Chem. Eur. J.* **2000**, *06*, 759.
[20] T. L. Chasse, C. B. Gorman, *Langmuir* **2004**, *20*, 8792.
[21] a) L. M. C. Beltran, J. R. Long, *Acc. Chem. Res.* **2005**, *38*, 325; b) M. Eddaoudi, D. Moler, H. Li, B. Chen, T. M. Reineke, M. O'Keeffe, O. M. Yaghi, *Acc. Chem. Res.* **2001**, *34*, 319.
[22] A. J. Tasiopoulos, A. Vinslava, W. Wernsdorfer, K. A. Abboud, G. Christou, *Angew. Chem.* **2004**, *116*, 2169; *Angew. Chem. Int. Ed.* **2004**, *43*, 2117.
[23] R. Shakya, C. Imbert, H. P. Hratchian, M. Lanznaster, M. J. Heeg, B. R. McGarvey, M. A. Allard, H. B. Schlegel, C. N. Verani, *Dalton Trans.* **2006**, 2517.
[24] C. Imbert, H. P. Hratchian, M. Lanznaster, M. J. Heeg, L. Hryhorczuk, B. R. McGarvey, H. B. Schlegel, C. N. Verani, *Inorg. Chem.* **2005**, *44*, 7414.
[25] a) M. Lanznaster, H. P. Hratchian, M. J. Heeg, L. Hryhorczuk, B. R. McGarvey, H. B. Schlegel, C. N. Verani, *Inorg. Chem.* **2006**, *45*, 955; b) M. Lanznaster, M. J. Heeg, G. T. Yee, B. R. McGarvey, C. N. Verani, *Inorg. Chem.* **2007**, *46*, 72.
[26] a) A. Mukherjee, R. Raghunathan, M. K. Saha, M. Nethaji, S. Ramasesha, A. R. Chakravarty, *Chem. Eur. J.* **2005**, *11*, 3087; b) F. Bramsen, A. D. Bond, C. J. McKenzie, R. G. Hazell, B. Moubaraki, K. S. Murray, *Chem. Eur. J.* **2005**, *11*, 3087; c) G. Aromí, J. Ribas, P. Gamez, O. Roubeau, H. Kooijman, A. L. Spek, S. Teat, E. MacLean, H. Stoeckli-Evans, J. Reedijk, *Chem. Eur. J.* **2004**, *10*, 6476.
[27] L. Chen, S. Breeze, R. Rousseau, S. Wang, L. Thompson, *Inorg. Chem.* **1995**, *34*, 454.
[28] W. E. Hatfield, J. A. Barnes, G. W. Inman, Jr., *Inorg. Chem.* **1971**, *10*, 1725.
[29] S. Teipel, K. Griesar, W. Haase, B. Krebs, *Inorg. Chem.* **1994**, *33*, 456.
[30] J. Reim, K. Griesar, W. Haase, B. Krebs, *J. Chem. Soc. Dalton Trans.* **1995**, 2649.
[31] M. Bera, W. Wong, G. Aromi, J. Ribas, D. Ray, *Inorg. Chem.* **2004**, *43*, 4787.
[32] S. Mukharjee, Th. Weyhermuller, E. Bothe, K. Weighard, P. Chaudhuri, *Eur. J. Inorg. Chem.* **2003**, 863.
[33] J. Reim, W. Werner, W. Haase, B. Krebs, *Chem. Eur. J.* **1998**, *4*, 289.
[34] M. Mikuria, K. Minowa, R. Nukada, *Bull. Chem. Soc. Jpn.* **2002**, *75*, 2595.
[35] V. McKee, S. Tandon, *J. Chem. Soc. Dalton Trans.* **1991**, 221.
[36] S. Breeze, S. Wang, L. Chen, *J. Chem. Soc. Dalton Trans.* **1996**, 1341.
[37] A. W. Addison, T. N. Rao, J. Reedjik, J. van Rijin, G. C. Verschoor *J. Chem. Soc. Dalton Trans.* **1984**, 1349. The τ value is a structural index that systematizes five-coordination geometries and is defined by $\tau=[\beta-\alpha/60°]$ with $\alpha=\beta=180°$ for a square pyramid ($\tau=0$, C_{4v}) and $\alpha=\beta<180°$ for a trigonal bipyramid ($\tau=1$, D_{3h}). The individual τ values of 0.011, 0.041, 0.103, and 0.076 were found, respectively, for Cu1, Cu2, Cu3, and Cu4.
[38] E. Ruiz, *Struct. Bonding* **2004**, *113*, 71, and references [82] and [83] therein.
[39] A. M. P. S. Goncalves da Silva, D. A. Armitage, R. G. Linford, *J. Colloid Interface Sci.* **1993**, *156*, 433.
[40] M. C. Petty, *Langmuir-Blodgett Films*, Cambridge University Press, Cambridge, **1996**, pp. 65–93.
[41] S. Kraus, D. Mandler, *Langmuir* **2006**, *22*, 7462.
[42] G. Williams, A. Soi, A. Hirsch, M. R. Bryce, M. C. Petty, *Thin Solid Films* **1993**, *230*, 73.
[43] a) S. Di Bella, S. Sortino, S. Conoci, S. Petralia, S. Casilli, L. Valli, *Inorg. Chem.* **2004**, *43*, 5368; b) M. C. Petty, *Langmuir–Blodgett Films*, Cambridge University Press, Cambridge, **1996**, pp. 32–37, and references therein.
[44] a) K. Wang, M. Haga, M. D. Hossain, H. Shindo, K. Hasebe, H. Monjushiro, *Langmuir* **2002**, *18*, 3528; b) M. Haga, N. Kato, H. Monjushiro, K. Wang, M. D. Hossain, *Supramol. Sci.* **1998**, *5*, 337.
[45] a) A. D. Becke, *J. Chem. Phys.* **1993**, *98*, 5648–5652; b) J. P. Perdew, Y. Wang, *Phys. Rev. B* **1992**, *45*, 13244.
[46] H. P. Hratchian, H. B. Schlegel in *Theory and Applications of Computational Chemistry: The First Forty Years* (Eds.: C. E. Dykstra, G. Frenking, K. S. Kim, G. E. Scuseria), Elsevier, Amsterdam, **2005**, p. 195.
[47] Gaussian 03 (Revision B.05), M. J. Frisch, G. W. Trucks, H. B. Schlegel, G. E. Scuseria, M. A. Robb, J. R. Cheeseman, J. A. Montgomery Jr., T. Vreven, K. N. Kudin, J. C. Burant, J. M. Millam, S. S. Iyengar, J. Tomasi, V. Barone, B. Mennucci, M. Cossi, G. Scalmani, N. Rega, G. A. Petersson, H. Nakatsuji, M. Hada, M. Ehara, K. Toyota, R. Fukuda, J. Hasegawa, M. Ishida, T. Nakajima, Y. Honda, O. Kitao, H. Nakai, M. Klene, X. Li, J. E. Knox, H. P. Hratchian, J. B. Cross, C. Adamo, J. Jaramillo, R. Gomperts, R. E. Stratmann, O. Yazyev, A. J. Austin, R. Cammi, C. Pomelli, J. W. Ochterski, P. Y. Ayala, K. Morokuma, G. A. Voth, P. Salvador, J. J. Dannenberg, V. G. Zakrzewski, S. Dapprich, A. D. Daniels, M. C. Strain, O. Farkas, D. K. Malick, A. D. Rabuck, K. Raghavachari, J. B. Foresman, J. V. Ortiz, Q. Cui, A. G. Baboul, S. Clifford, J. Cioslowski, B. B. Stefanov, G. Liu, A. Liashenko, P. Piskorz, I. Komaromi, R. L. Martin, D. J. Fox, T. Keith, M. A. Al-Laham, C. Y. Peng, A. Nanayakkara, M. Challacombe, P. M. W. Gill, B. Johnson, W. Chen, M. W. Wong, C. Gonzalez, J. A. Pople, Gaussian, Inc., Pittsburgh, PA, **2004**.
[48] R. Seeger, J. A. Pople, *J. Chem. Phys.* **1977**, *66*, 3045.

Received: June 8, 2007
Published online: October 23, 2007

